energies

MDPI

*Article*

# Energetic Assessment of SCWG Experiments with Reed Canary Grass and Ethanol Solution on Laboratory and Pilot Scale

**Julian Dutzi *, Nikolaos Boukis and Jörg Sauer**

Institute of Catalysis Research and Technology (IKFT), Karlsruhe Institute of Technology (KIT), 76344 Eggenstein-Leopoldshafen, Germany
* Correspondence: julian.dutzi@kit.edu; Tel.: +49-721-6082-8813

**Abstract:** The energetic assessment of biomass conversion processes is important for evaluating their application potential. Process energy efficiency is often evaluated based on simulation results for processes under idealized conditions. The present work uses data from a laboratory plant to perform an evaluation of the supercritical water gasification (SCWG). For this purpose, experiments were conducted with two types of feedstock, Reed Canary Grass and ethanol. Under the present lab-plant configuration, a cold gas efficiency of up to 79% could be reached, which is comparable to the gasification of biomass in fluidized-bed gasifiers or entrained-flow gasifiers. Based on the obtained data on the produced substances and their distribution, a scale up to pilot plant size was conducted. A model was derived from the available data to energetically assess different SCWG plant sizes based on real laboratory results. This model can be transferred to other feedstocks and other process designs to approximate the optimal size for the used biomass feedstock. The importance of heat recuperation in this process is described in detail based on pilot-scale data.

**Keywords:** supercritical water; biomass; gasification; scale up

**Citation:** Dutzi, J.; Boukis, N.; Sauer, J. Energetic Assessment of SCWG Experiments with Reed Canary Grass and Ethanol Solution on Laboratory and Pilot Scale. *Energies* **2023**, *16*, 6848. https://doi.org/10.3390/en16196848

Academic Editor: Gianluca Cavalaglio

Received: 26 August 2023
Revised: 22 September 2023
Accepted: 25 September 2023
Published: 27 September 2023



## 1. Introduction

Supercritical water gasification (SCWG) is a process that converts organic materials into a gas by exposing them to supercritical water that has been heated and pressurized beyond its critical point ($T > 374$ °C, $p > 22.1$ MPa) [1]. In this state, water no longer behaves as a liquid or a gas, but rather as a unique supercritical fluid [2]. Due to the characteristics of supercritical water, organics dissolve well in it [3,4]. Thus, the organic material is rapidly decomposed in the supercritical water via hydrolyzation reactions, producing a mixture of hydrogen, carbon dioxide, carbon monoxide, and methane, along with small amounts of other gases [5–8]. One of the major advantages of supercritical water gasification is that it can process a wide variety of organic materials, including agricultural waste and sewage sludge without the need for extensive pre-treatment [9–11]. This makes it a potentially useful tool for waste management and resource recovery.

However, supercritical water gasification is a demanding process. SCWG was proposed in the late 1970s by M. Modell, who conducted the first experiments on glucose conversion via SCWG [12]. Despite years of research, no commercial SCWG systems have been developed until now. Laboratory-scale experiments use different types of reactors, including batch reactors (e.g., autoclaves), tube reactors, and stirred-tank reactors [9,13]. There are several pilot-scale plants operating globally, including the VERENA plant at the Karlsruhe Institute of Technology, which is the first pilot plant for SCWG, and has a capacity of 100 kg $h^{-1}$ of feed slurry [7,14]. In the Netherlands, an industrial plant that is able to process 16 t $h^{-1}$ of waste per hour is being engineered [15].

The calculation of the energy consumption of conversion technologies is important in order to be able to compare them with existing technologies in terms of production costs and profitability. In the literature, little information is available on the energetic

assessment of SCWG plants. Boukis et al. described the energy flow for the gasification of ethanol and methanol solution at pilot scale based on experimental results [14,16,17]. Others have derived the efficiency of the SCWG process from simulations under idealized assumptions, such as thermodynamic equilibrium state [18–21]. In general, these assessments have been conducted for pilot-scale or even larger plants. This is usually reasonable for industrial applications, but there are cases where small plants are useful. In the context of the H2020 project CERESiS (ContaminatEd land Remediation through Energy crops for Soil improvement to liquid fuel Strategies), relatively small contaminated sites are to be freed from contaminants via phytoremediation [22]. In one of the investigated cases, the area is smaller than 10,000 $m^2$, and corresponds to six tons of dry biomass per year. The subsequently contaminated biomass can be processed via SCWG [23–25]. In this way, the organic matter can be decomposed, the inorganic contaminants can be separated, and a syngas is obtained from the biomass. This syngas can be converted into pure $H_2$, synthetic natural gas, or even Fischer–Tropsch fuel after further purification steps [22]. Since relatively small amounts of biomass are available, small SCWG plants are necessary for continuous operation.

In the present work, the lab-scale operation of an SCWG plant (throughput of up to 0.7 kg $h^{-1}$ feed) is assessed regarding product distribution and energy demand for the gasification of the model substances. A theoretical scaling up of the mass and energy balances to pilot scale was performed using the lab-scale results and the results reported by Boukis et al. for the gasification of ethanol solution at pilot scale [7]. A simple model is proposed to calculate the energy balances of continuous SCWG processes with laboratory data as reference. In this way, the present work can serve as a basis for the future design of SCWG plants. Additionally, the importance of heat recuperation in this process is described by analyzing the heat exchanger installed in the pilot SCWG plant at KIT.

## 2. Materials and Methods

### *2.1. Preparation of Educts for Laboratory Experiments*

For the lab-scale experiments, Reed Canary Grass (RCG) was used as biomass. It was provided as a powder (grain size < 0.25 mm) with a dry matter content of 97.4 wt.% (97.4 kg dry matter/100 kg feed) by the University of Strathclyde [26]. The elemental composition of the dry matter was 48.9 wt.% C, 35.9 wt.% O, 7.46 wt.% H and 0.09 wt.% S. A feed slurry was created by adding distilled water so that a dry matter content of 8 wt.% was achieved. Additionally, potassium hydrogen carbonate $KHCO_3$ (CAS: 298-14-6; purity ≥ 99%), supplied by VWR chemicals, was added as a homogeneous catalyst (5000 mg $K^+$/kg feed slurry) and 0.5 wt.% (0.5 kg xanthan/100 kg feed slurry) xanthan (E-415; CAS: 11138-66-2), supplied by Carl Roth GmbH, was added as thickener to prevent phase separation. The addition of $KHCO_3$ improves the water gas shift reaction, resulting in a higher production of $H_2$ [27–29].

In addition to the experiments with Reed Canary Grass, ethanol solution was gasified in the laboratory unit. Ethanol absolute (CAS: 64-17-5; purity: 99.97%), supplied by VWR chemicals, was mixed with distilled water to set an ethanol concentration of 6 wt.%.

### *2.2. Apparatus*

The lab-scale experiments were conducted with the continuous-flow plant LENA (German acronym for "Laboratory Plant for Energetic Utilization of Agricultural Materials"). The LENA plant is a high-pressure (up to 30 MPa) and high-temperature (up to 700 °C) plant. In the setup considered for the following energetic and economic assessment, the plant consisted of a preheater and two gasification reactors, as shown in Figure 1 and Table 1. The heating of the lab plant was electric.

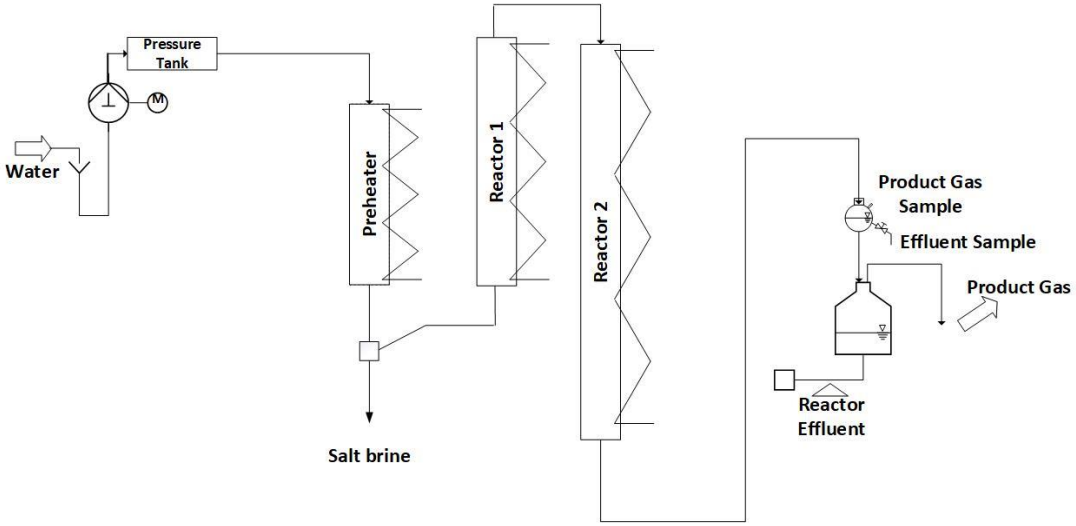


**Figure 1.** Schematic diagram of the LENA plant.

**Table 1.** Dimensions of the preheater and reactors.

| | Preheater | Reactor 1 | Reactor 2 |
|---|---|---|---|
| Material | SS316 with SS316 liner | Inconel 625 | Inconel 625 |
| Length/mm | 1200 | 1100 | 1800 |
| Inner diameter/mm | 3.2 | 8.0 | 8.0 |
| Electric heating | 5 spiral heaters | 3 rod heaters + 1 spiral heater | 6 rod heaters + 1 spiral heater |

SS316: Stainless steel 316.

In the preheater, the feed slurry is heated so that supercritical temperatures of water are reached. At a T-fitting downstream of the preheater, salts are supposed to be separated into the salt brine due to their low solubility in supercritical water [30] and due to gravity. The salt brine is ejected from the system into a container by a high-pressure valve that opens the pipe in which the salt brine is primarily collected at defined intervals for a short time (20 ms) to atmospheric pressure. The organics in the reaction mixture are transported sideways to the two SCWG reactors (two reactors to increase the residence time in the temperature zone above 600 °C) and gasified. The reactor effluent that leaves the second reactor is collected in a collection container.

### *2.3. Analysis*

Gas samples from a product gas are examined with a gas chromatograph (5890 series II plus, Hewlett Packard Inc.) in which a fused silica capillary column (Carboxen 1010 PLOT 30 m, made by SUPELCO) is installed. Thermal conductivity and flame ionization detectors are utilized to determine the volume fractions of different gas components such as $H_2$, CO, $CH_4$, $CO_2$, $C_2H_4$, $C_2H_6$, $C_3H_8$ and $C_3H_6$. The sampling process is carried out every 0.5 h.

At regular intervals, liquid samples are gathered from the effluent streams for the analysis of Total Carbon (TC) via combustion and Total Inorganic Carbon (TIC) through acid extraction using a *TOC* analyzer (DIMATOC 2100, produced by DIMATEC). By subtracting TIC from TC, Total Organic Carbon (*TOC*) is calculated. Trace elements, including Al, Ca, Cd, Cr, Cu, Fe, K, Mg, Mn, Mo, Na, Ni, Pb, S, Si, and Zn, are identified via Inductively Coupled Plasma–Optical Emission Spectrometry (ICP-OES) using an Agilent 725 spectrometer (by Agilent Technologies, Santa Clara, CA, USA).

A sample of the biomass feed is dried at 105 °C in an oven for 24 h, and afterwards, the C, H, N, and S contents are analyzed in the element analyzer vario EL cube (by Elementar Analysensysteme GmbH), and the trace elements are analyzed via ICP-OES.

### *2.4. Methods of Scaling and Energetic Assessment Study*

Data produced at laboratory scale that provide the chemical composition of the SCWG products are combined with literature data about the energetic performance of SCWG pilot plants with setups similar to that of the investigated laboratory plant to evaluate the SCWG process for the biomasses chosen in this study. Additionally, unpublished data on the measured temperatures of the heat exchanger from an experiment performed at the pilot plant scale are given.

The total mass and the mass of carbon and potassium, being the major compounds, are balanced for the laboratory experiments performed in this study. Minor compounds (e.g., sodium or sulfur) are not balanced, since they are not relevant for the energetic balance of the process. The mass balances of the laboratory experiments serve as a basis for the energetic assessment of the laboratory SCWG plant. The lower heating value of the product gas is calculated and compared to the lower heating value of the feed material to determine the efficiency of the process. Furthermore, the heating value of the other products (salt brine, reactor effluent, solid residue) is estimated based on the respective organic carbon content to assess the heat losses of the SCWG plant.

For scale up, the product distribution (total mass, carbon, potassium) is assumed to be independent of the SCWG plant size, and canbe directly transferred to a larger scale. Thus, the heating value based on the mass of the products remains the same. For a first scale-up, a pilot scale (throughput of 100 kg $h^{-1}$) is chosen, since data about heat losses and the required energy input in such a system have been published previously [7], and can be adjusted for the newly investigated feed materials.

To scale to larger sizes, model equations, which are displayed in detail in Section 3.3., are used to derive a simple model that takes into account that heat losses do not scale linearly with SCWG plant size.

### *2.5. Data Interpretation*

The following key figures are defined to evaluate the gasification experiments.

The degree of purity of the effluent can be measured using the *TOC* conversion $TOC_{conv}$, which compares the amount of *TOC* present in the effluent streams to that of the feed (as shown in Equation (1)). Any remaining *TOC* that is not found in the effluent streams may have been converted into gaseous products, dissolved inorganic compounds or solid deposits within the system.

$$TOC_{conv} = 1 - \frac{\dot{m}_{R,effluent} * TOC_R + \dot{m}_{S,effluent} * TOC_S}{\dot{m}_{Feed} * \alpha} \quad (1)$$

$\dot{m}_{R,effluent}$, Mass flow of reactor effluent (g/h) [SI: 2.778 × $10^{-7}$ kg/s]
$\dot{m}_{S,effluent}$, Mass flow of salt brine (g/h) [SI: 2.778 × $10^{-7}$ kg/s]
$TOC_R$, *TOC* content of reactor effluent ($mg_c/kg_{effluent}$) [SI: 1 × $10^{-6}$ $kg_c/kg_{effluent}$]
$TOC_S$, *TOC* content of salt brine ($mg_c/kg_{brine}$) [SI: 1 × $10^{-6}$ $kg_c/kg_{brine}$]
$\alpha$, *TOC* concentration in the feed (wt.%) [in SI: 1 × $10^{-2}$ $kg_c/kg_{Feed}$]

To quantify the efficiency of the gasification, the carbon efficiency *CE* and the gasification efficiency *GE* are defined as follows:

$$CE = \frac{\sum \beta_i * x_i * \frac{\dot{V}_{Gas} * p}{R * T} * M_c}{\dot{m}_{Feed} * \alpha} \quad (2)$$

$x_i$, Concentration of component '$i$' in the gas product (vol.%) [SI: 1 × $10^{-2}$ mol/mol]
$\beta_i$, Number of carbon atoms of component '$i$' in the gas product

$\dot{m}_{Feed}$, Feed mass flow (g/h) [SI: 2.778 × $10^{-7}$ kg/s]
$M_c$, Atomic mass of carbon (g/mol) [SI: 1 × $10^{-3}$ kg/mol]
$p$, Pressure (Pa)
$R$, Universal constant of gases (J/(K*mol))
$T$, Temperature (K)
$\dot{V}_{Gas}$, Gas flow under ambient conditions (L/h) [SI: 2.778 × $10^{-7}$ $m^3$/s]

$$GE = \frac{\sum x_i * \frac{\dot{V}_{Gas} * p}{R * T} * M_i}{\dot{m}_{Feed} * \alpha} \quad (3)$$

$M_i$, Atomic mass of component 'i' (g/mol) [SI: 1 × $10^{-3}$ kg/mol]

For the energetic assessment of the process, the cold gas efficiency is defined. This compares the lower heating value (*LHV*) of the product gas with the *LHV* of the used feed, in this case, RCG and ethanol.

$$\eta_{Coldgas} = \frac{\dot{m}_{Gas} * LHV_{Gas}}{\dot{m}_{organics} * LHV_{organics}} \quad (4)$$

$$LHV_{Gas} = \sum x_i * \dot{V}_{Gas} * LHV_i \quad (5)$$

$LHV_i$, Volumetric lower heating value of species 'i' ($J/m^3$)
$\dot{m}$, Mass flow (g/h) [SI: 2.778 × $10^{-7}$ kg/s]

For better readability and understanding of the different sizes of the SCWG units investigated, units other than the SI base units were used (e.g., g $h^{-1}$ or kg $h^{-1}$).

## 3. Results

### *3.1. Lab-Scale Experiments*

Four SCWG experiments were conducted in the LENA lab plant: three with RCG and one with ethanol solution, as shown in Table 2. In all experiments with RCG, the reaction temperature was set to 650 °C, the pressure was 28 MPa and the throughput was 700 g $h^{-1}$. The only parameter that was varied in these experiments was the maximum preheating temperature, $T_{max,Preheater}$, to optimize salt separation. The preheater is responsible for heating the reaction medium to supercritical temperatures so that salts can be separated at the salt separation T-fitting. Potassium, as the predominant salt building element in the experiments with Reed Canary Grass, was separated poorly at the T-fitting. The potassium distribution was very similar for all experiments. Thus, the salt separation was not improved. It is presumed that the reaction temperature has a much greater influence on the gasification and the product distribution than the preheating temperature. Additionally, the experimental outcomes of these tests indicate that the preheating temperature does not significantly influence the product distribution and thus the energy balance, and thus the following mass balances and energy balances will be calculated using the results of experiment 1 (see Table 2). The experiment with ethanol was conducted under the same temperatures and pressure as the experiments with RCG, and the throughput was set to 250 g $h^{-1}$. One experiment was chosen for the evaluation of ethanol gasification, since the ethanol solution is gasified completely. Thus, the carbon is completely transferred to the gas phase and the carbon distribution in the products is always the same under similar conditions. For ethanol, this is the case under the chosen conditions, as can be seen in previous work [31]. The gas composition is influenced by catalysts added to the system and can vary. In the present experiment, no catalyst was added to the system, and thus thermodynamic equilibrium was not reached. Once potassium is added to the reaction the gas composition is changed, as shown in [31], and with that also the heating value of the product gas. As shown in this study, the calculations can easily be adjusted to new

feed materials and product gas compositions. Thus, the data originating from the experiment with ethanol solution are suitable for evaluating the process in general.

**Table 2.** Laboratory experiments conducted with Reed Canary Grass (RCG) and ethanol.

| Experiment Number | Biomass | $T_{max,Preheater}$ | CE | TOC-Conversion |
|---|---|---|---|---|
| | | °C | % | % |
| 1 | RCG | 500 | 65.8 | 86.0 |
| 2 | RCG | 570 | 66.7 | 85.4 |
| 3 | RCG | 400 | 63.4 | 86.0 |
| Mean values | | | 65.3 | 85.8 |
| 4 | Ethanol | 500 | 99.3 | 99.8 |

CE: carbon efficiency; $T_{max,Preheater}$: maximum preheating temperature; TOC: total organic carbon.

During the laboratory experiments with RCG, the following product fractions were formed (see also Figure 2):

- Product gas;
- Reactor effluent;
- Salt brine;
- Solid residue in the reaction system.

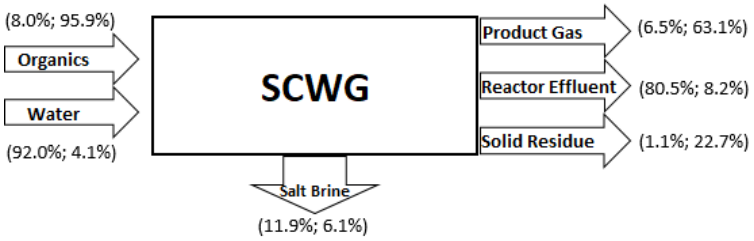


**Figure 2.** Mass balance of the lab-scale SCWG process for experiment 1 with RCG (mass%, carbon%).

In addition to the product gas, carbon is contained in other side products. Due to incomplete gasification (as shown in Table 2), the reactor effluent contains some carbon ($TOC_{effluent}$ = 3420 $mg_{TOC}/kg_{effluent}$, $TIC_{effluent}$ = 359 $mg_{TIC}/kg_{effluent}$). Longer residence times or higher reaction temperatures generally result in higher gasification efficiencies [32–36]. These are two measures that could be implemented in future experiments to further reduce the *TOC* content in the reactor effluent. In the context of the present process, salts are supposed to be separated after preheating the reaction mixture [25]. In the process of salt separation part of the organic feed is lost to the salt brine ($TOC_{salt\ brine}$ = 18,780 $mg_{TOC}/kg_{brine}$, $TIC_{salt\ brine}$ = 23 $mg_{TIC}/kg_{brine}$). This amounts to 6.1 wt.% of the carbon in the feed. Due to unwanted side reactions, solid residue mainly consisting of carbon and salts forms in the system. This solid residue can cause blockage of the flow [37,38], and thus needs to be avoided in industrial applications. If it cannot be separated during the continuous process, long-term operation is not possible. The formation of carbon-containing solid deposits could possibly be reduced by appying faster heating rates [38–40] or by dilution of the feed to lower biomass concentrations [13,34,41].

In Table 3, the total mass distribution and the distribution of carbon and potassium ($K^+$ only for RCG) are displayed. It is clear that in the case of RCG, 65.8 wt.% of the *TOC* is gasified. A total of 8.2 wt.% of the total carbon is still contained in the effluent. As described above, this amount could be reduced by using higher reaction temperatures or higher residence times. A total of 22.7 wt.% of the fed carbon is lost due to the formation of solid deposits. This poses a danger to continuous operation.

**Table 3.** Mass distribution of experiments with Reed Canary Grass and ethanol solution.

| | Reed Canary Grass | | | Ethanol | |
|---|---|---|---|---|---|
| **Mass Flow Rate** | **g/h** | **g/h C** | **g/h K+** | **g/h** | **g/h C** |
| **Feed** | **700.0** | **26.2** | **3.51** | **250.0** | **7.80** |
| Organics | 56.0 | 25.1[+] | - | 15.0 | 7.80 |
| Water | 644.0 | 1.08* | 3.51 | 235.0 | - |
| **Sum of products** | **700.0** | **26.2** | **3.51** | **250.0** | **7.80** |
| Gas | 45.3 | 16.5 | - | 15.9 | 7.78 |
| Reactor effluent | 562.9 | 2.14 | 0.13 | 234.1 | 0.02 |
| Solid residue | 8.77 | 5.95 | 2.82 | - | - |
| Salt concentrate | 83.0 | 1.59 | 0.56 | - | - |

C: carbon; K+: potassium. [+] The carbon contained in the organics is present in the form of *TOC* and can be gasified. * The carbon (in the form of TIC, which is not gasified) contained in the water in the feed is due to the addition of $KHCO_3$.

There is optimization potential regarding carbon efficiency, but also regarding salt separation. $KHCO_3$ is added as a homogeneous catalyst. During salt separation, potassium is only separated to 16 wt.%, and the other 84 wt.% is either contained in the effluent (4 wt.%) or forms a residue (80 wt.%) (see Figure 3). This needs to be addressed through improved salt separation. For the separation of salts, the preheating temperature is crucial. This is described in our previous publication [25].

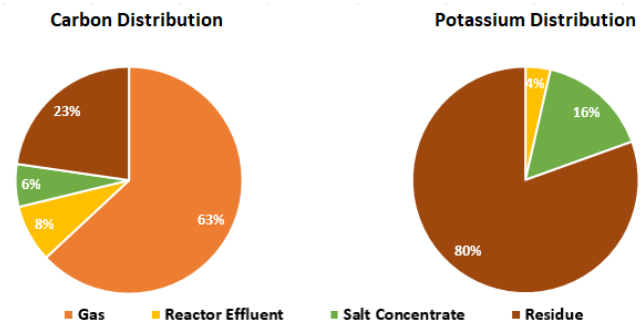


**Figure 3.** Mass distribution of experiments with RCG.

During the gasification of ethanol solution, no salt separation is needed, and thus no salt brine is produced. The carbon efficiency is CE = 99.8%, and the ethanol is completely gasified. No solids form in the system (solid residue), and thus the product fractions are reduced to product gas and reactor effluent. In the case of ethanol gasification, 99.8 wt.% of the carbon is contained in the product gas and only 0.2 wt.% is contained in the effluent. The gasification of ethanol is generally more effective and easier than the gasification of biomass due to the less complex structure. The ethanol molecule is easily decomposed with few intermediates [31,42,43]. During the decomposition of biomass, many intermediates are formed, some of which form solid deposits [3,10,44].

The described mass distribution serves as a basis for assessing the energy balance of the LENA lab plant when gasifying dry biomass and ethanol solution. In addition to the mass balance, the input of energy in form of electricity has to be taken into account (no other form of energy is put into the system). Sixteen electric heaters (750 W each) are installed, which are not operated at full power. The measured percentage of operation of the heaters amounts to 3.54 kW of electric heating for the RCG experiments and 1.95 kW for the ethanol experiments (the latter is lower due to the slower flow rate and thus the better heat transfer). Due to the electricity needed for the feed pump, a total of 3.69 kW of electricity input for the RCG experiments and 2.00 kW for the ethanol experiments is required.

The energy-containing solid residue is not present in the ethanol experiments. In experiment 1, the fed mass of RCG is equal to 0.28 kW of thermal energy (heating value of RCG = 3.97 kWh $kg^{-1}$). The product gas compositions and the lower heating value of the product gases are shown in Table 4. The product gas of the RCG gasification has a *LHV* of 0.15 kW and the gas of ethanol gasification has a *LHV* of 0.11 kW. Due to the high $CO_2$ content of the product gas when gasifying RCG, the *LHV* of the gas is only slightly higher than the *LHV* of the ethanol experiment, even though 41.4 L $h^{-1}$ is produced during the gasification of RCG (throughput 700 g $h^{-1}$) and only 20.4 L $h^{-1}$ of gas is produced during the gasification of ethanol solution (250 g $h^{-1}$ flow).

**Table 4.** Product gas composition and *LHV*.

| | ***LHV* [45]** | **Reed Canary Grass** | | **Ethanol** | |
|---|---|---|---|---|---|
| | | **Composition** | ***LHV*** | **Composition** | ***LHV*** |
| | **MJ/m³** | **vol.%** | **kW** | **vol.%** | **kW** |
| $H_2$ | 10.782 | 32.97 | $4.08 \times 10^{-2}$ | 37.92 | $2.32 \times 10^{-2}$ |
| CO | 12.634 | 0.340 | $4.93 \times 10^{-4}$ | 12.19 | $8.72 \times 10^{-3}$ |
| $CO_2$ | | 45.38 | | 15.21 | |
| $CH_4$ | 35.894 | 16.53 | $6.82 \times 10^{-2}$ | 27.27 | $5.54 \times 10^{-2}$ |
| $C_2H_4$ | 59.478 | 0.299 | $2.05 \times 10^{-3}$ | 0.057 | $2.02 \times 10^{-4}$ |
| $C_2H_6$ | 64.382 | 3.310 | $2.45 \times 10^{-2}$ | 7.351 | $2.68 \times 10^{-2}$ |
| $C_3H_6$ | 87.591 | 0.349 | $3.52 \times 10^{-3}$ | 0.000 | |
| $C_3H_8$ | 93.118 | 0.830 | $8.88 \times 10^{-3}$ | 0.006 | $5.28 \times 10^{-5}$ |
| | | | $1.48 \times 10^{-1}$ | | $1.14 \times 10^{-1}$ |

*LHV*: lower heating value.

During the experiments with RCG, there are two further product streams that contain chemically bound energy. As shown in Figure 3, 8 wt.% of TC of the feed is still contained in the effluent. It is also assumed that 8% of the heating value of the feed is contained in the effluent, since the *LHV* of the wastewater, salt brine and the solid residue is not exactly known. For experiment 1, this amounts to 0.024 kW. The amount of carbon in the solid residue is roughly three times as high as in the liquid effluent, and thus the energy content is about 0.066 kW. The difference between the mentioned input of electrical and thermal energy and the output in thermal energy can be assumed to be losses, mainly thermal losses. This is displayed in Table 5. In the case of RCG, 94% of the input energy is lost to thermal losses due to insufficient insulation and because no heat recuperation is installed.

**Table 5.** Energy balance of the lab plant for different feeds.

| | **Reed Canary Grass** | **Ethanol** |
|---|---|---|
| | **kW** | **kW** |
| Electricity | 3.72 | 2.03 |
| Feed | 0.28 | 0.11 |
| Gas | 0.15 | 0.11 |
| Reactor effluent | 0.02 | 0.00 |
| Solid residue | 0.07 | 0.00 |
| Losses | 3.76 | 2.03 |

In the case of ethanol, the losses are about the same (94.6%). The difference between the two feedstocks is the cold gas efficiency CGE. For RCG, the CGE is 53.3%, while for ethanol, it is 102.7%. The large difference arises from the difference in carbon efficiency, which is low for the RCG, while ethanol is gasified completely. CGE is greater than 100% for ethanol gasification. A possible reason for this could be the generation of $H_2$ from $H_2O$ in the process.

Theoretically, if no solids are formed during the gasification of RCG and no carbon is contained in the effluent, only the carbon contained in the salt brine will be lost (6 wt.% of carbon). The maximum reachable CE would thus be 94%, and therefore the amount of gas produced would rise to roughly 59 L $h^{-1}$ (*LHV* = 0.22 kW). The CGE could at maximum rise to 78.6% for RCG under the present reaction system configuration.

For biomass types like RCG, the comparison of SCWG and conventional gasification is interesting. The typical CGE of fluidized-bed gasifiers is in the range of 62 to 80% for fossil fuels [46]. For biomass, it has been shown that a CGE above 70% can be reached [46,47]. Entrained-flow gasifiers typically range from 69 to 81% in CGE (for fossil fuels) [46]. Compared to both kinds of conventional gasifier, the achieved CGE of 53.6% with RCG is low. As described above, avoiding solid formation could increase the CGE to roughly 79%. The operation of SCWG plants with little to no formation of solid deposits is possible, as has been shown by D'Jesus et al. (CE of up to 100% when gasifying corn silage) [36], and such high CGEs are thus achievable. For this, the process parameters have to be optimized and adjusted to the processed biomass. This comparison shows that when considering CGE, SCWG shows comparable efficiency to conventional gasification, and SCWG could thus be an alternative technology for the conversion of some biomasses.

### *3.2. Pilot-Scale Energy Calculation*

The calculated mass balance is scaled up to pilot scale (throughput 100 kg $h^{-1}$). To achieve this, it is assumed that the product distribution (shown in Table 3) does not change with scale up. For a 100 kg $h^{-1}$ plant, this amounts to the values (dry matter of RCG = 8 wt.%, ethanol concentration 6 wt.%) presented in Table 6.

**Table 6.** Mass balances for pilot-scale operation.

| | Reed Canary Grass | | | Ethanol | |
|---|---|---|---|---|---|
| **Mass Flow Rate** | **kg/h** | **kg/h C** | **kg/h K+** | **kg/h** | **kg/h C** |
| Feed | 100.0 | 3.7 | 0.5 | 100.0 | 3.1 |
| Organics | 8.0 | 3.6 | - | 6.0 | 3.1 |
| Water | 92.0 | 0.2 | 0.5 | 94.0 | - |
| Sum of products | 100.0 | 3.7 | 0.5 | 100.0 | 3.1 |
| Product gas | 6.5 | 2.4 | - | 6.4 | 3.0 |
| Reactor effluent | 80.4 | 0.3 | 0.0 | 93.7 | 0.1 |
| Solid residue | 1.3 | 0.9 | 0.4 | - | - |
| Salt concentrate | 11.9 | 0.2 | 0.1 | - | - |

C: carbon; K+: potassium.

The heating value of the feed input is 39.8 kW for RCG and 44.5 kW for ethanol. The produced gas has an *LHV* of 21.2 kW for RCG and 45.6 kW for ethanol. To perform an energetic assessment of a pilot plant, a sufficient data base is necessary, since losses and thus required heating do not scale linearly from laboratory size to pilot size due to changes in surface-to-volume ratio, increased insulation, and, most importantly, installed heat recuperation. For this purpose, the energetic assessment of the VERENA pilot plant at KIT, performed by Boukis et al., was used as a reference [7]. The setup of the VERENA pilot plant is very similar to the setup of the LENA lab plant, and thus the energy consumption and losses measured at the VERENA plant can be considered to be a suitable reference and can be adapted to the biomasses used in the present experiments. The main difference from the laboratory experiments described in Section 3.1 is the installed heat exchanger and better insulation. Boukis et al. processed 100 kg $h^{-1}$ of ethanol solution (14.4 wt.% of ethanol). The heat consumption (35 kW) and electricity input (8 kW) (mainly for the operation of the pumps and of the $CO_2$ scrubber) can be taken as a reference for a 100 kg $h^{-1}$ operation. In the present study, for the feed stream, the heating will be carried out electrically instead of burning product gas, since the product gas serves as a reactant for further

synthesis (Fischer–Tropsch) within the CERESiS project, and thus burning part of it is not reasonable [22]. Since not all heat can be recuperated within the heat exchanger, hot water leaves the system containing about 11 kW of thermal energy (at T = 155 °C).

The energy balance is shown in Table 7. Given the product distribution described in Section 3.1 (scaled-up values in Table 6), the *LHV* of the product gas amounts to 21.2 kW (see Table 7) (=26% of the input energy). The relative energy contained in the product gas is significantly higher than in the lab experiments described in the section above due to heat recuperation and better insulation. The gasification of 100 kg $h^{-1}$ ethanol solution produces 45.6 kW of product gas (see Table 7). This amounts to 52% of the input energy. The energy efficiency is lower in the present case then it was for Boukis et al., since they were able to gasify more ethanol (14.4 wt.%) with the same energy input. Thus, gasifying 6 wt.% of ethanol is energetically not sufficient, since higher concentrations could be gasified with the same energy input (same temperature, same power consumption of the pumps). A total of 30.9 kW is lost due to thermal losses in the case of ethanol gasification (no salt brine in the case of ethanol gasification). This fits the calculations of Boukis et al. very well [7].

**Table 7.** Energy balance of the pilot-scale SCWG process.

| | **Reed Canary Grass** | **Ethanol** |
|---|---|---|
| | **kW** | **kW** |
| Electricity | 8.0 | 8.0 |
| Heating (electric) | 35.0 | 35.0 |
| Feed | 39.8 | 44.5 |
| Gas | 21.2 | 45.6 |
| Reactor effluent | 3.4 | - |
| Solid residue | 9.4 | - |
| Hot water | 11.0 | 11.0 |
| Losses | 37.8 | 30.9 |

For operation with RCG, the thermal losses can be calculated as 37.8 kW, and thus are higher than those measured by Boukis et al. [7]. This is because the residual heat (roughly 5.0 kW) and the *LHV* of the organics (roughly 2.5 kW) contained in the salt brine are lost due to salt separation. Boukis et al. did not separate any salt brine during the gasification of ethanol solution. The losses due to salt separation and thermal losses of the lab plant are both included in the displayed "losses". The total losses account for 46% of the energy input for RCG. When additionally considering the solid deposits and the *TOC* in the effluent as losses, since they are unwanted side products, about 50.6 kW are lost.

It was demonstrated that with a sufficient data reference (in this case energetic assessment of VERENA plant), the assessment of the SCWG process can be adapted for other feedstocks with the help of laboratory experiments. Using this approach, a first estimation on the energy demand of the SCWG process for given biomasses can be conducted without the need for experiments at pilot scale.

### *3.3. Scale-Up Model Description*

The laboratory experiments with RCG presented some hurdles, especially the formation of solid residue, that need to be avoided or handled before a pilot or demonstration plant can be sufficiently operated. Nevertheless, laboratory experiments can generally serve as a reference for scale up as shown in Section 3.2. Based on the laboratory results (especially product distribution) and the energetic assessment of a 100 kg $h^{-1}$ pilot plant, assumptions can be made to further scale up the size of an SCWG plant. The following assumptions are made:

- The product distribution (shown in Table 3) is independent of plant size.

- The electricity for pumping liquids is proportional to the throughput. For a pump, the power consumption can be calculated according to Equation (6) (for conversion factors to basic SI units, see Section 2.5).

$$P = \frac{p * \dot{V}}{\eta_{Pump}} = \frac{p * V_{Pump} * n}{\eta_{Pump}} \quad (6)$$

$n$, Rotations per minute (1/min)
$p$, Pressure (MPa)
$P$, Power consumption of pump (kW)
$V_{Pump}$, Volume of pump (m³)
$\dot{V}$, Volume flow (m³/h)
$\eta_{Pump}$, Efficiency of pump (-)

- Thermal losses decrease proportionally with increasing plant size, since the surface-to-volume ratio increases with a factor of 2/3. Thus, the thermal losses can be approximated using the following equation:

$$Thermal\ losses = 37.8\ kW * \left(\frac{plant\ throughput\ \left(\frac{kg}{h}\right)}{100\ \frac{kg}{h}}\right)^{\left(\frac{2}{3}\right)} \quad (7)$$

Due to the relative decrease in losses, the required heating also decreases relative to the plant size. The electrical input needed for heating and operation of the plant can be calculated with Equation (8), since energy balance must be kept in the system.

$$\begin{aligned} Elec.Input(kW) = {} & Energy\ Output - Energy\ Input\ through\ Biomass \\ = {} & Losses + Thermal\ Energy\ in\ Products - Heating\ Value\ of\ Biomass \end{aligned} \quad (8)$$

The losses are calculated according to Equation (7) and the heating value of the BM is known. In Table 8, the resulting energy key parameters are shown.

**Table 8.** Energetic calculations for different scale-up sizes with Reed Canary Grass (8 wt.%).

| Plant throughput/kg h$^{-1}$ | 100 | 200 | 500 | 1000 |
|---|---|---|---|---|
| Biomass input/kW | 39.8 | 79.6 | 198.9 | 397.8 |
| Electricity input/kW | 43.0* | 70.4 | 135.6 | 227.6 |
| Product gas/kW | 21.2 | 42.4 | 106.0 | 212.0 |
| Thermal losses/kW | 37.8 | 60.0 | 110.4 | 175.3 |

* Taken from [7].

The amount of energy contained in the product gas relative to the energy input can be calculated according to Equation (9). With the help of Equation (8) and basic knowledge from laboratory experiments ($GE$ and gas composition) and knowledge about the biomass ($LHV_{BM,spez}$), the calculation can easily be adjusted according to the biomass input.

$$\frac{LHV_{Gas}}{Energy\ Input}(\%) = \frac{LHV_{Gas,spez} * \dot{m}_{Gas}}{elec.input\ + LHV_{BM}} = \frac{LHV_{Gas,spez} * \dot{m}_{BM} * GE}{elec.input\ + LHV_{BM,spez} * \dot{m}_{BM}} \quad (9)$$

$GE$, Gasification efficiency (%)
$LHV_i$, *LHV* of component '$i$' (kW)
$LHV_{i,spez}$, Specific *LHV* of component '$i$' (kWh/kg)

The *LHV* of the produced gas relative to the energy input grows according to a logarithmic trend with increasing plant size due to the dependency of thermal losses on plant size. The losses relative to the energy input decrease with a logarithmic trend (see Figure 4). According to this simplified consideration, the larger the SCWG plant gets, the better

it will be in terms of minimizing thermal losses. This behavior is independent of the feedstock used, and thus also applies to ethanol solutions.

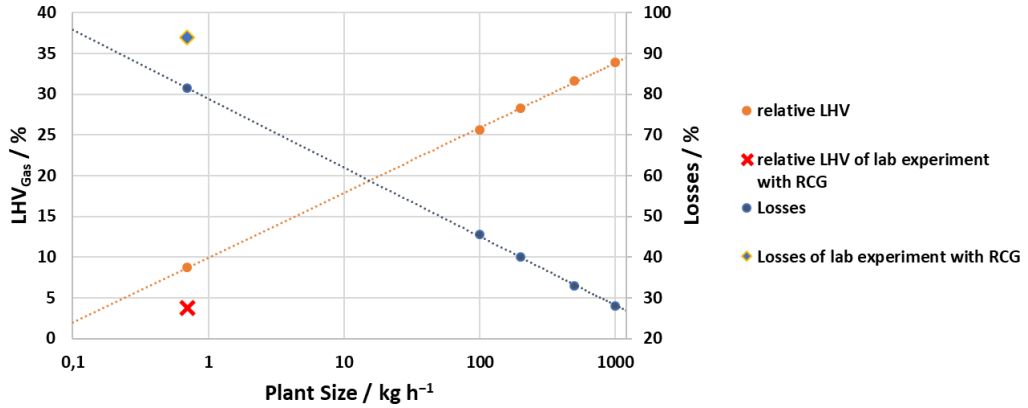


**Figure 4.** Lower heating value (*LHV*) of product gas and losses relative to energy input for scale up with Reed Canary Grass (RCG) based on Table 8 and Equation (9).

As shown in Figure 4, the model overestimates the energy contained in the product gas and underestimates the losses for a small laboratory plant. The main reason for this is (as described in Section 3.2) that in the LENA laboratory plant, no heat recuperation is performed, and the insulation is highly insufficient, unlike in the VERENA pilot plant that served as a reference for constructing this simplified method. The importance of the heat recuperation is described in detail in Section 3.4. On the other hand, industrial plants should be even better insulated, and the heat recuperation might also be better. Thus, the losses would decrease further. For a more detailed model, the energetic analysis of a real demonstration or industrial plant is necessary. This tool can serve as a basis for first evaluation of different plant sizes and most likely fits different pilot plant sizes the best. A tool like this fits well within the scope of the CERESiS project, where relatively small decentralized SCWG plants best fit the purpose of the project. Since the contaminated sites are far apart and of different sizes, different SCWG plants would need to be constructed.

### *3.4. VERENA Heat Exchanger*

As described in Section 3.2, the energy balance in this work is based on the measured energy consumption of the VERENA pilot plant at KIT. Boukis et al. measured the need for 35 kW of external heating for the operation of a 100 kg h$^{-1}$ with ethanol solution [7] at T = 600 °C to compensate heat losses, for example throughinsulation. To reach the reaction temperature, a much higher energy input would be needed if the residual heat of the product stream is not recuperated in a heat exchanger.

In the heat exchanger, the cold feed slurry is preheated by the heat taken from the product stream of the SCWG reactor. The cooling of the product stream would otherwise also be an energy-intensive process step. The heat exchanger is constructed as a double-pipe heat exchanger with an outer and an inner pipe. Usually, the inner pipe would contain the hot stream in such heat exchangers, and the outer pipe would contain the cold stream, in order to minimize the losses of heat to the environment. In the VERENA pilot plant this is not the case, due to precautions regarding the formation of blockages and the possibility to remove deposits. The inner pipes can be cleaned easily, while cleaning of the outer pipes is not possible. Thus, due to the higher risk of blocking of the feed containing pipe (due to high dry matter content and depending on the biomass a high inorganic content), the feed stream is directed through the inner pipes. The hot stream flows through the outer pipe, slightly increasing heat losses.

The heat exchanger contains nine layers of heat-exchanging pipes (horizontally mounted above each other). Each double pipe element has a length of 4.4 m. The inner pipe has an inner diameter of 8 mm and an outer diameter of 14.4 mm. The outer pipe has

an inner diameter of 18 mm and an outer diameter of 28 mm. To calculate the heat exchange surface, the middle of the inner pipe wall was chosen (diameter = 11 mm). Each pipe thus has an exchange surface of 0.152 m², amounting to 1.368 m² in total. The temperature data acquired for the experiment with ethanol solution (5 wt.% ethanol, throughput 80 kg $h^{-1}$) in the VERENA plant are depicted in Figure 5. The hot product stream enters the heat exchanger at a temperature of 584.5 °C and is cooled to 127.9 °C, while the feed stream is preheated from a temperature of 13.6 to 427.8 °C. Additionalheat-exchanging surface would have resulted in an increased preheating capability, but would also have increased the cost of building the preheater. Thus, only nine heat-exchanging pipes were installed. These data were measured using a cleaned heat exchanger. Nevertheless, it cannot be excluded that fouling was present on some levels.

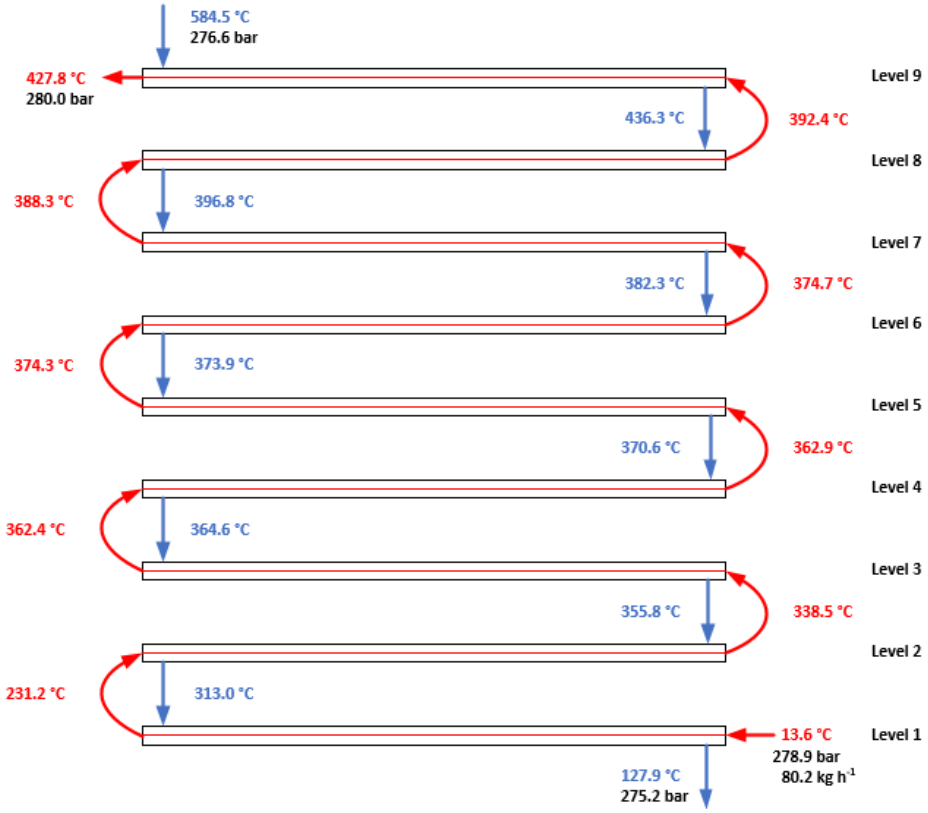


**Figure 5.** Temperature data from the VERENA heat exchanger (operation with 5 wt.% ethanol solution).

In order to calculate the heat that is transferred on each level, the heat capacity $c_p$ of water at a pressure of $p$ = 28 MPa is taken from the IAPWS-IF97 database of water and steam properties. The change in $c_p$ for different temperatures is displayed in Figure 6. For the calculation of energy absorbed by the feed stream and emitted by the hot product stream on each level, the heat capacity of both the feed slurry and the product mixture is assumed to be equal to the heat capacity of water, due to the high water content in the system of 95 wt.%. To calculate the amount of heat transferred, the mean heat capacity of each temperature interval (i.e., the difference between the inlet and outlet temperatures of one stream on one level) is calculated and used. The amount of emitted or absorbed heat is calculated according to Equation (10).

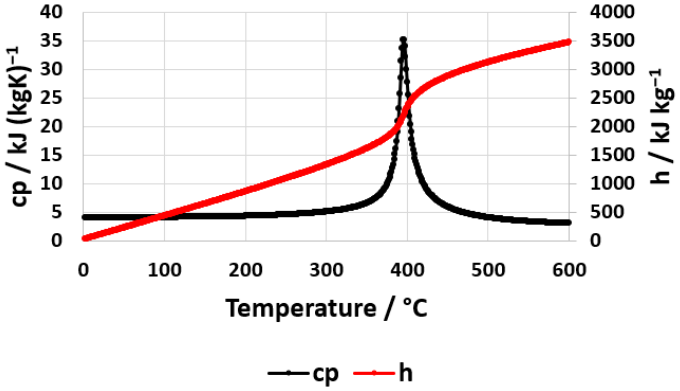


**Figure 6.** Heat capacity $c_p$ and specific heat h of water at $p$ = 28 MPa.

$$\dot{Q} = \dot{m} * \bar{c}_p * \Delta T \tag{10}$$

$\dot{Q}$, Heat stream (kW)
$\dot{m}$, Mass stream (kg/h)
$\bar{c}_p$, Mean heat capacity (kJ/(kg K))
$\Delta T$, Temperature difference (K)

The stream masses of the hot and cold streams are equal, since no salt separation occurs during the gasification of ethanol. The mean heat capacity and the calculated heat streams are displayed in Table 9. On levels 1 to 2, high amounts of heat are emitted from the hot fluid and transferred to the cold fluid due to the large temperature difference and the fact that liquid water is predominant in both streams. On levels 4 to 7, the temperatures in both parts of the pipes are quite similar (360 to 380 °C) (see Figure 7). Only small amounts of heat are transferred (see also Figure 6). On levels 8 and 9, the temperature differences between the inner and outer layers are large again, and a large amount of heat is transferred. The inner fluid takes up a total of 58.46 kW of heat from the outer fluid. The outer fluid releases 63.71 kW, thus leading to losses of 5.25 kW (8.2% of the released heat). To validate these calculations, the enthalpy difference between the inlet of the feed slurry and the outlet of the slurry in the preheater was calculated according to Equation (11) using the given example of the feed stream.

$$\Delta h = h_{out,Feed} - h_{in,Feed} = 2718.8\frac{kJ}{kg} - 80.6\frac{kJ}{kg} = 2638.2\frac{kJ}{kg} \tag{11}$$

$h$, Specific enthalpy of water (kJ/kg)

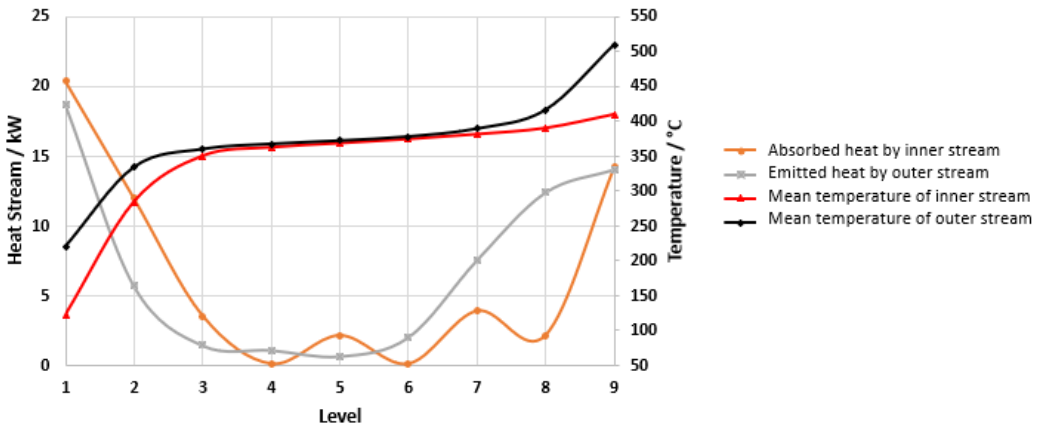


**Figure 7.** Heat emitted and absorbed on each level of the heat exchanger (operation with 5 wt.% ethanol).

**Table 9.** Key figures of the VERENA heat exchanger (operation with 5 wt.% ethanol solution).

| | Feed Stream (Inner Stream) | | | | Product Stream (Outer Stream) | | | |
|---|---|---|---|---|---|---|---|---|
| | $T_{in}$ °C | $T_{out}$ °C | $c_p(\bar{T})$ kJ (kg K)$^{-1}$ | $\dot{Q}$ kW | $T_{in}$ °C | $T_{out}$ °C | $c_p(\bar{T})$ kJ (kg K)$^{-1}$ | $\dot{Q}$ kW |
| Level 9 | 392.4 | 427.8 | 18.06 | 14.2 | 584.5 | 436.3 | 4.27 | −14.1 |
| Level 8 | 388.3 | 392.4 | 23.45 | 2.14 | 436.3 | 396.8 | 14.15 | −12.4 |
| Level 7 | 374.7 | 388.3 | 12.89 | 3.89 | 396.8 | 382.3 | 23.47 | −7.56 |
| Level 6 | 374.3 | 374.7 | 9.64 | 0.09 | 382.3 | 373.9 | 10.89 | −2.03 |
| Level 5 | 362.9 | 374.3 | 8.40 | 2.13 | 373.9 | 370.6 | 9.16 | −0.67 |
| Level 4 | 362.4 | 362.9 | 7.60 | 0.08 | 370.6 | 364.6 | 8.34 | −1.11 |
| Level 3 | 338.5 | 362.4 | 6.65 | 3.53 | 364.6 | 355.8 | 7.41 | −1.45 |
| Level 2 | 231.2 | 338.5 | 5.02 | 12.0 | 355.8 | 313.0 | 5.99 | −5.69 |
| Level 1 | 13.6 | 231.2 | 4.22 | 20.4 | 313.0 | 127.9 | 4.54 | −18.7 |
| Sum | | | | 58.5 | | | | −63.7 |

$T_{in}$: inlet temperature; $T_{out}$: outlet temperature; $c_p(\bar{T})$: heat capacity at mean temperature; $\dot{Q}$: absorbed/emitted heat.

By multiplying the specific enthalpy difference by the throughput of fluid, the amount of heat required can be calculated, with the results showing that 58.6 kW of heating is required and 63.6 kW of heat is released by the hot fluid. The difference between the two methods of calculation is much smaller than 1%.

To assess the influence of gas in the system (which is the case for the 5 wt.% ethanol solution), the displayed data are compared to operation with 80 kg h$^{-1}$ of pure water. In the case of water operation, salt separation was active. A total amount of 1.75 kg h$^{-1}$ of water is separated during this process. Thus, the flow of the hot stream is only 78.25 kg h$^{-1}$, instead of 80.00 kg h$^{-1}$. The hot stream enters the heat exchanger at a temperature of 578 °C and is cooled to 67 °C. The cold stream enters the heat exchanger at a temperature of 11 °C and is heated to 470 °C (see Figure 8).

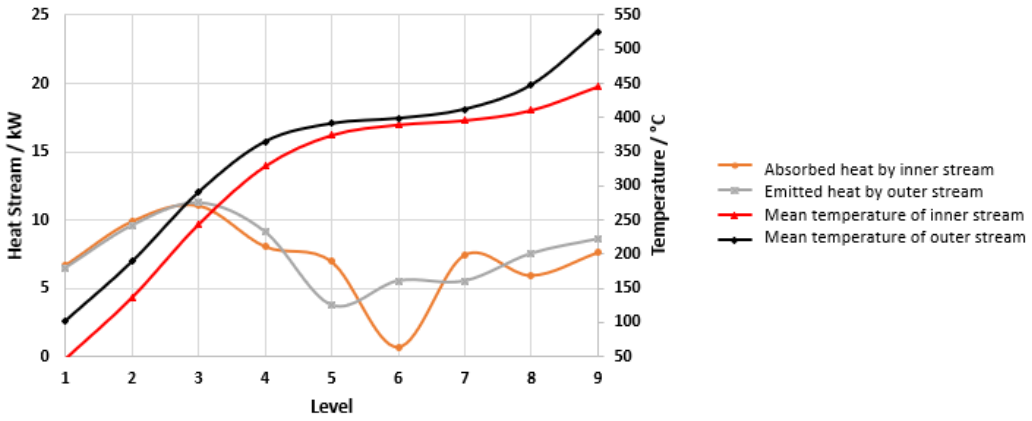


**Figure 8.** Emitted and absorbed heat on each level of the heat exchanger (operation with pure water).

In both cases, the temperature barely changes on multiple levels. This is due to the large changes in heat capacity and enthalpy in the temperature range of 370 to 420 °C (see Figure 6). Thus, a large amount of transferred heat is needed to increase the temperature. Due to the large heat capacity, small inaccuracies in temperature measurement can lead to errors in the calculation of transferred heat. For this reason, for operation with pure water as the feedstock (Figure 8), the calculated adsorbed heat is higher than the emitted heat on levels 5 and 7, while the absorbed heat on level 6 is much lower than the emitted heat. The gaseous compounds in the product of operation with ethanol decrease the heat

capacity of the stream, thus leading to a longer zone in which the temperature barely rises (levels 3 to 7) compared to the operation with water (levels 5 to 7).

When comparing the total transferred heat, it becomes clear that the heat transfer is more efficient when processing pure water. In the case of water, the outer stream releases 67.31 kW of heat and the inner stream absorbs 64.45 kW. This results in 2.86 kW of losses (4.3% of the released heat). The transferred amount of heat is greater, and fewer losses occur than when operating with ethanol solution. This results in better preheating in the case of water (478 °C instead of 428 °C with ethanol solution). Additionally, the hot product stream is cooled more efficiently in the case of operation with water (67 °C end temperature compared to 128 °C in the case of ethanol solution). The heat transfer coefficient $k$ can be calculated according to Equation (12) (with the use of Equation (13)). The transferred amount of heat $\dot{Q}$ is equal to the heat absorbed by the inner stream.

$$k = \frac{\dot{Q}}{A * \Delta T_{log}} \tag{12}$$

$A$, Heat exchanging surface (m²)
$\Delta T_{log}$, Logarithmic temperature difference (K)

$$\Delta T_{log} = \frac{\Delta T_{inner\ Pipe} - \Delta T_{outer\ Pipe}}{\ln\left(\frac{\Delta T_{inner\ Pipe}}{\Delta T_{outer\ Pipe}}\right)} \tag{13}$$

$\Delta T$, Temperature difference (K)

The resulting k-values are displayed in Table 10. Due to the errors in the calculation of transferred heat (as described above), especially, the mean k-value is of great importance. The mean k-value is much higher for the operation of water due to the higher total amount of heat transferred. At subcritical temperatures, the usual values of the heat transfer coefficient are between 300 to 1400 W (m² K)$^{-1}$ in double-pipe heat exchangers when both fluids are liquids [48]. This fits the calculated values of levels 1 to 4 very well, where subcritical temperatures occur in both pipes. Around the pseudo-critical point of water, the heat transfer coefficient rises to very high numbers—2140 W (m² K)$^{-1}$ for ethanol solution and 3413 W (m² K)$^{-1}$ for pure water. This phenomenon is due to the severe changes in the thermo-physical properties of water, such as heat conductivity and heat capacity, and has been described by other authors [49–51]. Heat transfer rates are enhanced in that region. The ethanol present in the feed and the gas that was formed by gasifying ethanol significantly decreases the heat transfer coefficients. An additional phenomenon could be that ethanol is already partially decomposed in endothermic reactions at temperatures below 400 °C. This would also reduce the maximum achievable preheating temperature. When designing a heat exchanger for an SCWG plant, performing calculations based on water can provide a good estimate, but the addition of organics to the feed and thus the gas in the product stream reduces the transferable amount of heat, resulting in a larger heat exchanger being required.

**Table 10.** Calculated k-values of ethanol and water operation.

| | $k_{Ethanol\text{-}Operation}$ W $(m^2K)^{-1}$ | $k_{Water\text{-}Operation}$ W $(m^2K)^{-1}$ |
|---|---|---|
| Level 9 | 1175.4 | 671.4 |
| Level 8 | 899.3 | 1206.9 |
| Level 7 | 1823.7 | 3412.7 |
| Level 6 | 214.5 | 1143.7 |
| Level 5 | 2140.9 | 3011.1 |
| Level 4 | 250.8 | 987.7 |
| Level 3 | 1537.9 | 695.9 |
| Level 2 | 1122.3 | 629.4 |
| Level 1 | 668.2 | 608.8 |
| Mean | 1092.5 | 1374.2 |

k: Heat transfer coefficient.

## 4. Conclusions

The mass and energy balance of continuous laboratory SCWG experiments was described in detail. With the energetic assessment of a pilot plant available, the scaling up of the SCWG process was demonstrated with the help of laboratory results. A simplified model was derived that can be used to approximate the thermal losses and the needed heating of SCWG plants at different sizes. For a more detailed model, the energetic assessment of a real demonstration plant would be necessary. Additionally, the importance of heat recuperation in the process of SCWG was demonstrated with experimental data acquired in a pilot SCWG plant.

The results obtained in the laboratory have shortcomings. However, they can be used as a first basis for the design of the pilot plant. The conversion of the biomass was incomplete, and some solids were formed in the process. These obstacles need to be overcome for sufficient continuous operation of any SCWG plant. Possible ways were suggested in this paper. The described method of energetic assessment can easily be adjusted to improved results . The energetic assessment, including the scaling up, can also easily be adjusted to different feedstocks with only a laboratory experiment needed.

**Author Contributions:** Conceptualization, J.D. and N.B.; methodology, N.B.; validation, J.D., N.B. and J.S.; formal analysis, J.D.; investigation, J.D.; resources, N.B.; data curation, J.D.; writing—original draft preparation, J.D.; writing—review and editing, N.B. and J.S.; visualization, J.D.; supervision, J.S.; funding acquisition, N.B. All authors have read and agreed to the published version of the manuscript.

**Funding:** This research work was funded by the H2020 EU-Project CERESiS (Grant-Agreement-Nr.: 101006717).

**Data Availability Statement:** Not applicable.

**Acknowledgments:** The authors would like to thank E. Hauer for the contributions to the experimental work and K. Weiss, who was responsible for most of the mechanical work, for the contributions during the lab-scale experiments. Special thanks to the University of Strathclyde for providing the biomassReed Canary Grass. The authors would like to thank D. Katsourinis and A. Rentizelas for the coordination of the H2020 project CERESiS. We would like to thank the operation team of the VERENA plant, who performed the pilot plant experiments, especially U. Galla, H. Lam and S. Henecka. We also acknowledge support by the KIT Publication Fund of the Karlsruhe Institute of Technology.

**Conflicts of Interest:** The authors declare no conflict of interest.

## References

1. Kaltschmitt, M.; Hartmann, H.; Hofbauer, H. *Energie aus Biomasse*, 2nd ed.; Springer: Berlin/Heidelberg, Germany, 2009; ISBN 978-3-540-85094-6.
2. Gadhe, J.B.; Gupta, R.B. Hydrogen Production by Methanol Reforming in Supercritical Water: Suppression of Methane Formation. *Ind. Eng. Chem. Res.* **2005**, *44*, 4577–4585. https://doi.org/10.1021/ie049268f.

3. Kruse, A. Supercritical water gasification. *Biofuels Bioprod. Bioref.* **2008**, *2*, 415–437. https://doi.org/10.1002/bbb.
4. Loppinet-Serani, A.; Aymonier, C.; Cansell, F. Current and Foreseeable Applications of Supercritical Water for Energy and the Environment. *ChemSusChem: Chem. Sustain. Energy Mater.* **2008**, *1*, 486–503. https://doi.org/10.1002/cssc.200700167.
5. Kruse, A.; Funke, A.; Titirici, M. Hydrothermal conversion of biomass to fuels and energetic materials. *Curr. Opin. Biotechnol.* **2013**, *17*, 515–521. https://doi.org/10.1016/j.cbpa.2013.05.004.
6. Boukis, N.; Stoll, I.K. Gasification of Biomass in Supercritical Water, Challenges for the Process Design—Lessons Learned from the Operation Experience of the First Dedicated Pilot Plant. *Processes* **2021**, *9*, 455. https://doi.org/10.3390/pr9030455.
7. Boukis, N.; Galla, U.; Müller, H.; Dinjus, E. Die VERENA-Anlage–Erzeugung von Wasserstoff aus Biomasse. *Gülzower Fachgespräche Band 25 Wasserstoff aus Biomasse;* Fachagentur Nachwachsende Rohstoffe e.V: Gülzow, Germany, 2006; pp. 115–127.
8. Susanti, R.F.; Veriansyah, B.; Kim, J.-D.; Kim, J.; Lee, Y.-W. Continuous supercritical water gasification of isooctane: A promising reactor design. *Int. J. Hydrog. Energy* **2010**, *35*, 1957–1970. https://doi.org/10.1016/j.ijhydene.2009.12.157.
9. Möbius, A.; Boukis, N.; Sauer, J. Gasification of biomass in supercritical water (SCWG). In *Materials and Processes for Energy: Communicating Current Research and Technological Developments*; Formatex Research Center: Jody Road Norristown, PA, USA, 2013; ISBN 978-84-939843-7-3.
10. Yakaboylu, O.; Harnick, J.; Smit, K.G.; Jong, W. Supercritical Water Gasification of Biomass: A Literature and Technology Overview. *Energies* **2015**, *8*, 859–894. https://doi.org/10.3390/en8020859.
11. Boukis, N.; Galla, U.; Müller, H.; Dinjus, E. Behaviour of inorganic salts during hydrothermal gasification of biomass. In Proceedings of the 17th European Biomass Conference and Exhibition, Hamburg, Germany, 29 June–3 July 2009.
12. Modell, M.; Reid, R.C.; Amin, S.I. Gasifiaction Process. Patent US05/742,712, 12 September 1978.
13. Okolie, J.A.; Rana, R.; Nanda, S.; Dalai, A.K.; Kozinski, J.A. Supercritical water gasification of biomass: A state-of- the-art review of process parameters, reaction mechanisms and catalysis. *Sustain. Energy Fuels* **2019**, *3*, 578–598. https://doi.org/10.1039/c8se00565f.
14. Boukis, N.; Galla, U.; Diem, V.; D'Jesús Montilva, P.; Dinjus, E. Hydrogen generation from wet biomass in supercritical water. In Proceedings of the 2nd World Conference on Biomass for Energy, Industry and Climate Protection, Rome, Italy, 10–14 May 2004.
15. National Hydrothermal Gasification Working Group. *Hydrothermal Gasification–White Paper*; National Hydrothermal Gasification Working Group: Bois-Colombes, France, 2023.
16. List, K.; Boukis, N.; Ackermann, R. Hydrothermal Gasification of biomass vs. anaerobic fermentation–technology assessment under ecological aspects. In Proceedings of the 15th European Biomass Conference & Exhibition, Berlin, Germany, 7–11 May 2007.
17. Boukis, N.; Kruse, A.; Galla, U.; Diem, V.; Dinjus, E. Biomassevergasung in überkritischem Wasser. *Nachrichten–Forschungszentrum Karlsr.* **2003**, *35*, 99–104.
18. Macri, D.; Catizzone, E.; Molino, A.; Migliori, M. Supercritical water gasification of biomass and agro-food residues: Energy assessment from modelling approach. *Renew. Energy* **2020**, *150*, 624–636. https://doi.org/10.1016/j.renene.2019.12.147.
19. Chen, J.; Liang, J.; Xu, Z.; Jiaqiang, E. Assessment of supercritical water gasification process for combustible gas production from thermodynamic, environmental and techno-economic perspectives: A review. *Energy Convers. Manag.* **2020**, *226*, 113497. https://doi.org/10.1016/j.enconman.2020.113497.
20. Magdeldin, M.; Kohl, T.; de Blasio, C.; Järvinen, M. Heat Integration Assessment for the Conceptual Plant Design of Synthetic Natural Gas Production from Supercritical Water Gasification of Spirulina Algae. In Proceedings of the Ecos 2015–The 28th International Conference on Fficiency, Cost, Optimization, Simulation and Environmental Impact of Energy Systems, Pau, France, 30 June–3 July 2015.
21. Magdeldin, M.; Kohl, T.; Järvinen, M. Process modeling, synthesis and thermodynamic evaluation of hydrogen production from hydrothermal processing of lipid extracted algae integrated with a downstream reformer conceptual plant. *Biofuels* **2016**, *7*, 97–116. https://doi.org/10.1080/17597269.2015.1118785.
22. CERESiS Consortium. CERESiS–ContaminatEd land Remediation through Energy crops for Soil improvement to liquid biofuel Strategies. Available online: https://ceresis.eu/ (accessed on 28 January 2023).
23. Su, W.; Liu, P.; Cai, C.; Ma, H.; Jiang, B.; Xing, Y.; Liang, Y.; Cai, L.; Xia, C.; Le, Q.V.; et al. Hydrogen production and heavy metal immobilization using hyperaccumulators in supercritical water gasification. *J. Hazard* **2021**, *402*, 123541. https://doi.org/10.1016/j.jhazmat.2020.123541.
24. Li, J.; Chen, J.; Chen, S. Supercritical water treatment of heavy metal and arsenic metalloid-bioaccumulating-biomass. *Ecotoxicol. Environ. Saf.* **2018**, *157*, 102–110. https://doi.org/10.1016/j.ecoenv.2018.03.069.
25. Dutzi, J.; Boukis, N.; Sauer, J. Process Effluent Recycling in the Supercritical Water Gasification of Dry Biomass. *Processes* **2023**, *11*, 797. https://doi.org/10.3390/pr11030797.
26. Lord, R.A. Reed canarygrass (Phalaris arundinacea) outperforms Miscanthus or willow on marginal soils, brownfield and non-agricultural sites for local, sustainable energy crop production. *Biomass Bioenergy* **2015**, *78*, 110–125. https://doi.org/10.1016/j.biombioe.2015.04.015.
27. Sinag, A.; Kruse, A.; Schwarzkopf, V. Key Compounds of the Hydropyrolysis of Glucose in Supercritical Water in the Presence of $K_2CO_3$. *Ind. Eng. Chem. Res.* **2003**, *42*, 3516–3521. https://doi.org/10.1021/ie030079r.

28. Zhu, Z.; Toor, S.S.; Rosendahl, L.A.; Yu, D.; Chen, G. Influence of alkali catalyst on product yield and properties via hydrothermal liquefaction of barley straw. *Energy* **2015**, *80*, 284–292. https://doi.org/10.1016/j.energy.2014.11.071.
29. Yoshida, T.; Oshima, Y.; Matsumura, Y. Gasification of biomass model compounds and real biomass in supercritical water. *Biomass Bioenergy* **2004**, *26*, 71–78. https://doi.org/10.1016/S0961-9534(03)00063-1.
30. Schubert, M.; Regler, J.W.; Vogel, F. Continuous salt precipitation and separation from supercritical water. Part 1: Type 1 salts. *J. Supercrit. Fluids* **2010**, *52*, 99–112. https://doi.org/10.1016/j.supflu.2009.10.002.
31. Dutzi, J.; Vadarlis, A.A.; Boukis, N.; Sauer, J. Comparison of Experimental Results with Thermodynamic Equilibrium Simulations of Supercritical Water Gasification of Concentrated Ethanol Solutions with Focus on Water Splitting. *Ind. Eng. Chem. Res.* **2023**, *62,* 12501–12512. https://doi.org/10.1021/acs.iecr.3c01595.
32. Yakaboylu, O.; Albrecht, I.; Harnick, J.; Smit, K.G.; Tsalidis, G.-A.; Marcello, M.D.; Anastasakis, K.; Jong, W. de. Supercritical water gasification of biomass in fluidized bed: First results and experiences obtained from TU Delft/Gensos semi-pilot scale setup. *Biomass Bioenergy* **2018**, *111*, 330–342. https://doi.org/10.1016/j.biombioe.2016.12.007.
33. Promdej, C.; Matsumura, Y. Temperature Effect on Hydrothermal Decomposition of Glucose in Sub–And Supercritical Water. *Ind. Eng. Chem. Res.* **2011**, *50*, 8492–8497. https://doi.org/10.1021/ie200298c.
34. D'Jesus, P. Die Vergasung von Realer Biomasse in Überkritischem Wasser: Untersuchung des Einflusses von Prozessvariablen und Edukteigenschaften. PhD. Thesis; Universität Karlsruhe, Karlsruhe, Germany, 2007.
35. D'Jesus, P.; Boukis, N.; Kraushaar-Czarnetski, B.; Dinjus, E. Gasification of corn and clover grass in supercritical water. *Fuel* **2006**, *85*, 1032–1038. https://doi.org/10.1016/j.fuel.2005.10.022.
36. D'Jesus, P.; Boukis, N.; Kraushaar-Czarnetski, B.; Dinjus, E. Influence of Process Variables on Gasification of Corn Silage in Supercritical Water. *Ind. Eng. Chem. Res.* **2006**, *45*, 1622–1630. https://doi.org/10.1021/ie050367i.
37. Boukis, N.; Galla, U. Verfahren zur Hydrothermalen Vergasung von Biomasse in Überkritischem Wasser. Patent DE102006044116B3, 28 February 2008.
38. Guo, L.; Cao, C.; Lu, Y. Supercritical Water Gasification of Biomass and Organic Wastes. In *Biomass;* IntechOpen: London, UK, 2010; ISBN 978-953-307-113-8.
39. Tushar, M.; Dutta, A.; Xu, C. Effects of Reactor Wall Properties, Operating Conditions and Challenges for SCWG of Real Wet Biomass. In *Near-Critical and Supercritical Water and Their Applications*: *Biofuels and Biorefineries 2*; Fang, Z., Xu, C., Eds.; Springer Science + Business Media Dordrecht: Dordrecht, The Netherlands, 2014; pp 207–229, ISBN 978-94-017-8922-6.
40. Kruse, A.; Henningsen, T.; Sinag, A.; Pfeiffer, J. Biomass Gasification in Supercritical Water: Influence of the Dry Matter Content and the Formation of Phenols. *Ind. Eng. Chem. Res.* **2003**, *42*, 3711–3717. https://doi.org/10.1021/ie0209430.
41. Nanda, S.; Reddy, S.N.; Hunter, H.N.; Dalai, A.K.; Kozinski, J.A. Supercritical water gasification of fructose as a model compound for waste fruits and vegetables. *J. Supercrit. Fluids* **2015**, *104*, 112–121. https://doi.org/10.1016/j.supflu.2015.05.009.
42. Arita, T.; Nakahara, K.; Nagami, K.; Kajimoto, O. Hydrogen generation from ethanol in supercritical water without catalyst. *Tetrahedron Lett.* **2003**, *44*, 1083–1086. https://doi.org/10.1016/S0040-4039(02)02704-1.
43. Therdthianwong, S.; Srisiriwat, N.; Therdthianwong, A.; Croiset, E. Hydrogen production from bioethanol reforming in supercritical water. *J. Supercrit. Fluids* **2011**, *57*, 58–65. https://doi.org/10.1016/j.supflu.2011.02.005.
44. Waldner, M.H.; Vogel, F. Renewable Production of Methane from Woody Biomass by Catalytic Hydrothermal Gasification. *Ind. Eng. Chem. Res.* **2005**, *44*, 4543–4551. https://doi.org/10.1021/ie050161h.
45. Cerbe, G. *Grundlagen der Gastechnik*, 6th ed., vollständig neu bearbeitete Auflage; Carl Hanser Verlag: Munchen, Germany, 2004, ISBN 3-446-22803-9.
46. Reimert, R.; Marschner, F.; Renner, H.-J.; Boll, W.; Supp, E.; Brejc, M.; Liebner, W.; Schaub, G. Gas Production, 2. Processes. In *Ullmann's Encyclopedia of Industrial Chemistry*; Wiley-VCH: Weinheim, Germany, 2011; ISBN 9783527303854.
47. Jamin, N.A.; Saleh, S.; Samad, N.A. Influences of Gasification Temperature and Equivalence Ratio on Fluidized Bed Gasification of Raw and Torrefied Wood Wastes. *Chem. Eng. Trans.* **2020**, *80*, 127–132. https://doi.org/10.3303/CET2080022.
48. Roetzel, W.; Spang, B. *Wärmedurchgang*. In *VDI-Wärmeatlas: Berechnungsblätter für den Wärmeübergang*; Springer: Berlin/Heidelberg, Germany, 2013; ISBN 978-3-642-19980-6.
49. Huang, X.; Wang, Q.; Song, Z.; Yin, Y.; Wang, H. Heat transfer characteristics of supercritical water in horizontal double-pipe. *Appl. Therm. Eng.* **2020**, *173*, 115191. https://doi.org/10.1016/j.applthermaleng.2020.115191.
50. Bazargan, M.; Fraser, D. Heat Transfer to Supercritical Water in a Horizontal Pipe: Modeling, New Empirical Correlation, and Comparison Against Experimental Data. *J. Heat Transf.* **2009**, *131*, 61702. https://doi.org/10.1115/1.3082403.
51. Swenson, H.S.; Carver, J.R.; Kakarala, C.R. Heat Transfer to Supercritical Water in Smooth-Bore Tiles. *J. Heat Transf.* **1965**, *87*, 477–483. https://doi.org/10.1115/1.3689139.